communications biology

A Nature Portfolio journal

Article

https://doi.org/10.1038/s42003-025-08856-5

Immediate-early genes Arc and c-Fos show divergent brain-wide expression following contextual fear conditioning

Nicholas E. Bulthuis [1], Liliette I. Quintana [2,5], Michelle Stackmann[1,6] & Christine A. Denny [3,4]

Encoding or retrieving a fear memory induces activity across the entire brain. Neurons involved in these processes are often identified by the expression of immediate-early genes (IEGs), but the extent to which the patterns of this expression correspond between IEGs has not been well characterized. Here, male mice were administered either context exposure (no shock) or 3-shock contextual fear conditioning and euthanized 1 h after encoding, retrieval 1 day later, or retrieval 5 days later. Brain tissue was immunostained for Arc and c-Fos protein, and expression was quantified across several brain regions. We find that expression of the two IEGs substantially diverges, with fewer than 50% of total labeled cells expressing both markers across memory states. Furthermore, memory state broadly influences Arc$^+$ but not c-Fos$^+$ cell density in select regions. These results suggest that the ensembles identified by each gene may be more anatomically and functionally distinct than commonly thought.

Learning or remembering a fearful experience requires the coordinated activity of thousands of neurons across the brain[1–3]. This brain-wide cellular trace is termed an engram, memory trace, or neural correlate of a memory, and it is defined as the ensemble of neurons active during both memory encoding and retrieval that is hypothesized to underlie memory storage[4–7]. Indeed, engrams in the hippocampus (HPC), amygdala (AMG), and other brain regions have functional significance: neurons active during contextual fear conditioning (CFC) in mice can later be stimulated to drive retrieval in the absence of learned contextual cues[8,9] or inhibited to prevent retrieval in a conditioned context[10].

The systems developed to tag and identify engrams take advantage of immediate-early genes (IEGs), a class of genes expressed in neurons at low basal levels, but which are rapidly and transiently expressed upon neural activity. IEGs include a variety of transcription factors (TFs), intracellular signaling molecules, and postsynaptic proteins, and they contribute in various ways to synaptic plasticity, cell maintenance, and memory formation[11,12]. Engram-tagging strategies use promoters for select IEGs to drive expression of transgenic constructs, which are combined with drug-inducible systems like Cre-loxP recombination or tetracycline transactivator (tTA)- tetracycline response element (TRE)/Tet-Off transcriptional controls to enable temporally-precise capture of active neurons. When paired with a single-trial learning paradigm like CFC, IEG-based tools can identify the engram of conditioned fear as the overlap between the populations of cells tagged during initial foot shock (memory encoding) and cells expressing IEGs shortly following context re-exposure (memory retrieval), as assessed by in situ hybridization or immunohistochemistry.

Despite the widespread use of IEGs as activity markers, the correspondence between the expression patterns of even the most commonly used IEGs has not been fully characterized across multiple memory states. One such IEG, c-Fos, encodes a TF that binds with other TFs such as JunB to form the AP-1 complex. Expression of c-Fos is induced by increased intracellular concentrations of cyclic adenosine monophosphate (cAMP) and Ca^{2+} via the mitogen-activated protein kinase (MAPK) signaling pathway, which activates TFs such as cAMP response element-binding protein (CREB), Elk-1, and serum response factor (SRF)[13,14]. *c-Fos* mRNA is detectable in neurons within minutes[15] of learning-evoked activity[16], and c-Fos protein levels peak approximately 1 h after behavior or artificial electroconvulsive stimulation[17].

Another commonly used IEG, *Arc/Arg3.1* (*Arc*), encodes an effector protein that serves multiple functions in several regions of an active neuron. Arc was first discovered to be trafficked from the nucleus to synaptically-active segments of dendrites[18,19], where *Arc* mRNA is translated locally[20] and Arc protein is involved in AMPA receptor (AMPAR) trafficking[21,22]. Interestingly, however, Arc also functions in the nucleus to regulate transcription of the AMPAR subunit GluA1 to control cell-wide synaptic strength[23]. The expression of Arc can be driven by multiple distinct signaling

[1]Doctoral Program in Neurobiology and Behavior (NB&B), Columbia University, New York, NY, USA. [2]Department of Neuroscience and Behavior, Barnard College, New York, NY, USA. [3]Division of Systems Neuroscience, Research Foundation for Mental Hygiene, Inc. (RFMH) / New York State Psychiatric Institute (NYSPI), New York, NY, USA. [4]Department of Psychiatry, Columbia University Irving Medical Center (CUIMC), New York, NY, USA. [5]Present address: Department of Pediatrics, Weill Cornell Medicine, New York, NY, USA. [6]Present address: Department of Neurobiology, Stanford University School of Medicine, Stanford, CA, USA.
e-mail: cad2125@cumc.columbia.edu

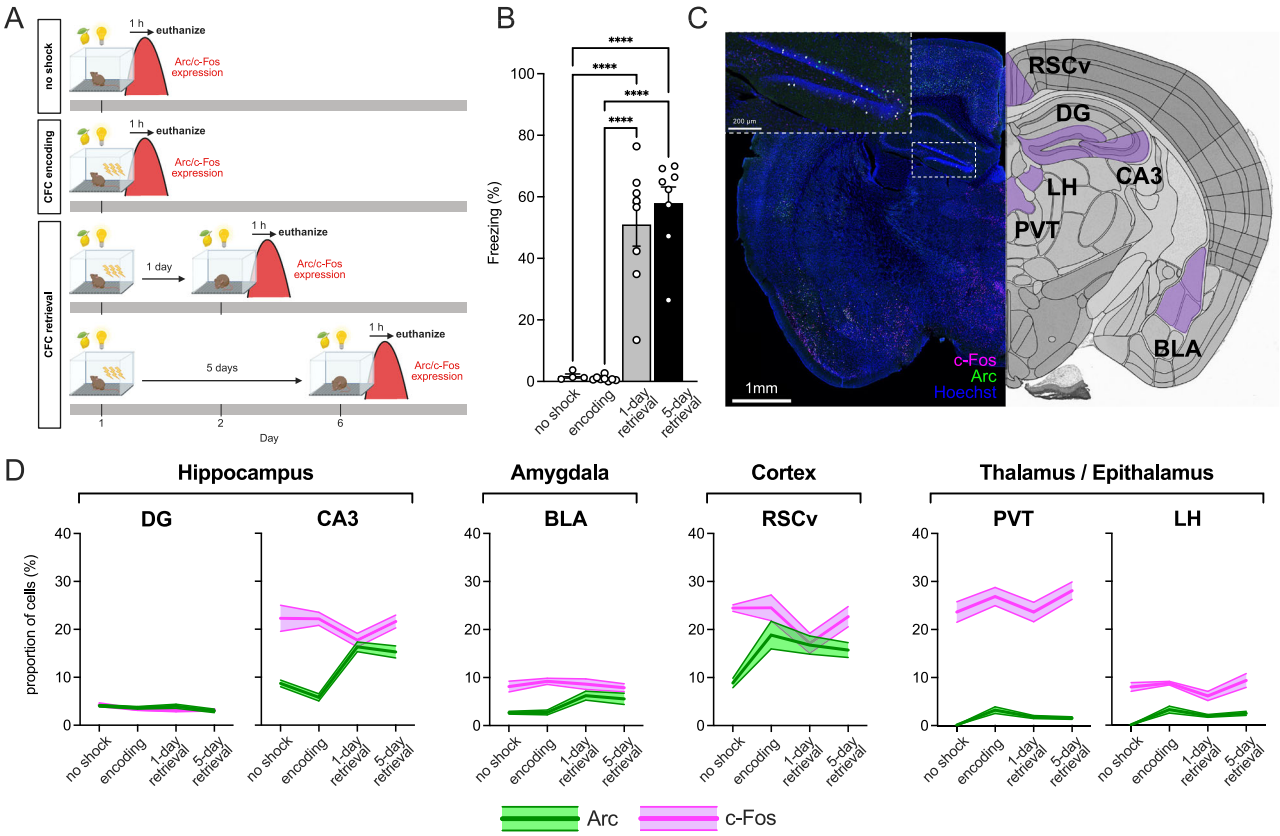

Fig. 1 | Arc and c-Fos are differentially expressed across numerous quantified brain regions. A Experimental timeline and conditions. Red indicates transient expression of IEGs Arc and c-Fos following behavior-driven neuronal activity. **B** Percentage of time spent freezing was greater in 1-day and 5-day retrieval groups compared to no shock and encoding groups. **C** Left: representative coronal hemisphere section showing Arc (green) and c-Fos (magenta) expression with a Hoechst nuclear counterstain (blue). Right: schematic coronal hemisphere section showing quantified brain regions (purple), adapted from the Allen Mouse Brain Atlas (Mouse, P56) at http://atlas.brain-map.org[83]. **D** Expression levels of Arc (green) and c-Fos (magenta) as measured by percentage of all cells per region expressing each marker. Group means are represented by the thick inner line; SEM are represented by thin outer lines. N = 4 (no shock) or 8 (encoding, 1-day retrieval, 5-day retrieval) mice. Error bars indicate ±SEM. ****$p < 0.0001$. DG dentate gyrus, BLA basolateral amygdala complex, RSCv ventral retrosplenial cortex, PVT paraventricular nucleus of the thalamus, LH lateral habenula. **A** was created in BioRender. Bulthuis, N. (2025) https://BioRender.com/ih5c2sa.

factors, including MAPK[24], CREB, SRF[25], and myocyte enhancer factor 2 (MEF2), which interact with a region termed the synaptic activity-responsive element (SARE) in the *Arc* promoter[26]. Functionally, Arc has been shown to play a crucial role in memory encoding, as its inhibition has been shown to impair long-term potentiation (LTP)[27,28] (though see also Kyrke-Smith et al.[29]), and *Arc* knockout (KO) mice retain intact short- but not long-term memory[30]. Akin to c-Fos, *Arc* mRNA is detected rapidly following behavior, within minutes after spatial exploration[31] or context memory[32], and Arc protein levels peak between 1 and 4 h following electroconvulsive stimulation[17]. Lastly, Arc protein has also been shown to form viral-like capsids that transport *Arc* mRNA from neuron to neuron[33], though the function of this novel phenomenon is not yet fully elucidated.

Here, we sought to determine how Arc and c-Fos are differentially affected by learning state by examining their simultaneous expression both temporally and spatially: across multiple states of fear memory in numerous brain regions. Male mice were administered either a control context exposure without shock or a 3-shock CFC paradigm and euthanized 1 h after (1) no shock, (2) CFC encoding, (3) CFC retrieval 1 day later, or (4) CFC retrieval 5 days later, after which brain tissue was processed and immunostained for Arc and c-Fos. Both 1-day and 5-day retrieval timepoints were used to determine if the length of time elapsed from memory encoding to retrieval influences IEG expression. Brain areas analyzed included subregions of the HPC, such as the dentate gyrus (DG) and CA3, which are involved in contextual memory and pattern separation[34,35]; the basolateral amygdala complex (BLA), involved in fear conditioning, extinction, and consolidation[36,37]; the ventral retrosplenial cortex (RSCv), involved in spatial, contextual, and cue-specific memory[38,39] and linked to age- and disease-related cognitive decline[40,41]; the ventral anterior cingulate cortex (ACAv), a region of the dorsomedial prefrontal cortex (dmPFC), involved in cognitive functions including long-term memory[42]; and thalamic/epithalamic regions the paraventricular nucleus of the thalamus (PVT), involved in salience processing and fear expression[43,44], and the lateral habenula (LH), involved in aversive behavior and learning[45]. We found that the expression of Arc and c-Fos is both region- and memory state-dependent, with dynamic shifts of Arc expression across time in CA3 and greater c-Fos than Arc expression in numerous quantified brain areas. Our results suggest that multiple experimental variables differentially influence IEG expression, and they provide essential context for how analyses of Arc or c-Fos as a neural activity marker should be interpreted.

Results

Arc and c-Fos are simultaneously expressed during contextual fear conditioning encoding and retrieval

Here, CFC was used to test the effect of memory state on the induction of Arc and c-Fos. Mice were administered either a no shock control or 3-shock CFC and euthanized 1 h following no shock, encoding, 1-day retrieval, or 5-day retrieval to capture Arc and c-Fos protein expression induced at each timepoint (Fig. 1A). As expected, mice froze significantly more during memory retrieval than no shock or encoding, indicating successful

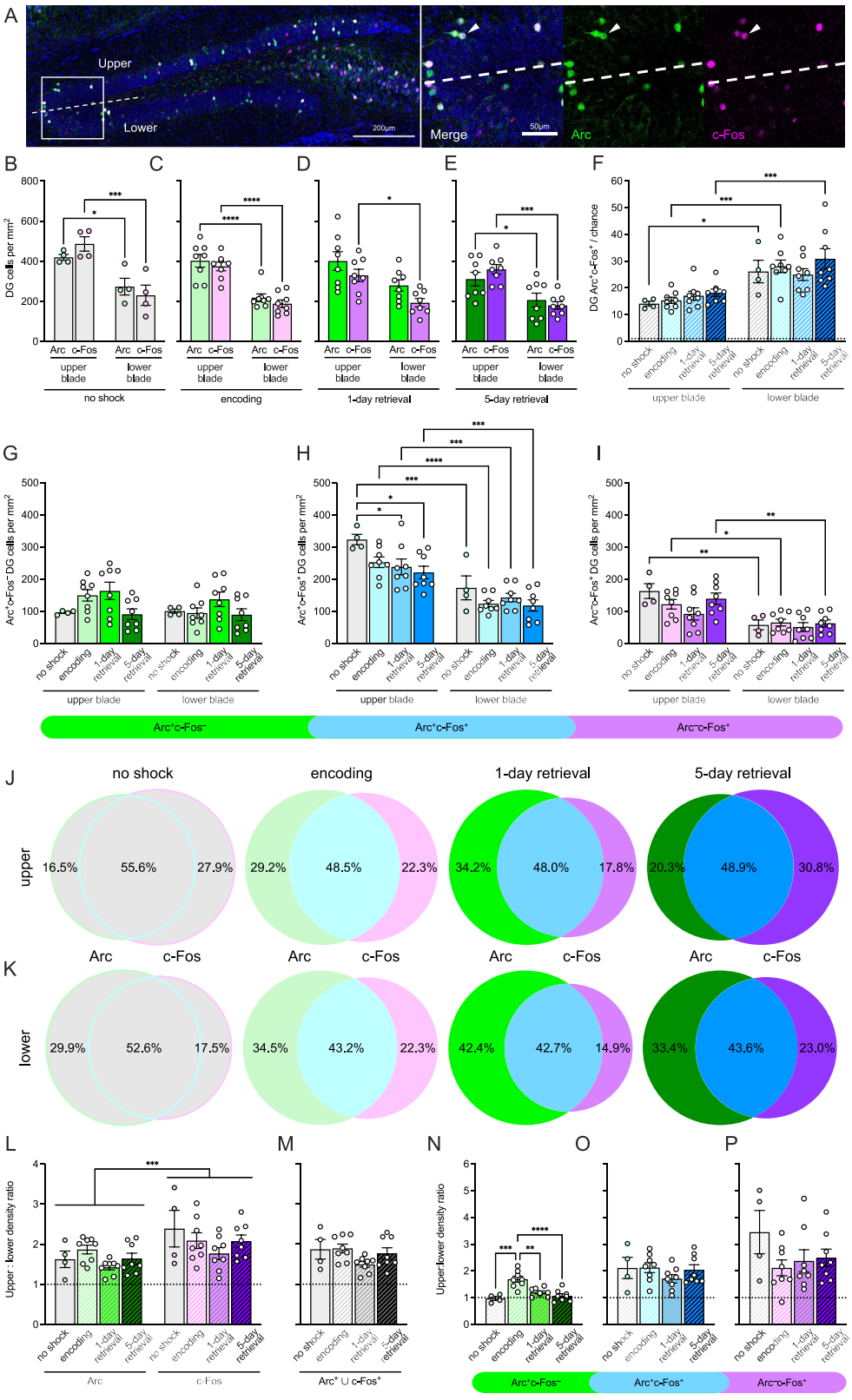

expression of the contextual fear memory (Fig. 1B). To visualize Arc and c-Fos proteins simultaneously, several immunohistochemical protocols were first tested to identify the combination of antibodies that provided the most robust labeling with the least discernible cross-reactivity between channels (Fig. S1). Our optimized strategy leveraged rabbit anti-Arc and rat anti-c-Fos primary antibodies to reduce nonspecific binding, enabling quantification of Arc$^+$ and c-Fos$^+$ cells in hippocampal, cortical, and subcortical regions of fixed brain tissue slices (Fig. 1C). This approach determined that up to 30% of all cells in each region expressed each gene at each timepoint (Fig. 1D).

Fig. 2 | Arc and c-Fos expression patterns diverge at all memory states in the DG. **A** Left: Arc (green) and c-Fos (magenta) expression; Hoechst nuclear counterstain (blue). Right: inset. White arrow: example $Arc^+c\text{-}Fos^+$ cell. **B**–**E** Arc^+ and $c\text{-}Fos^+$ cell densities in the upper blade were greater than those in the lower blade during no shock, encoding, and 5-day retrieval. At 1-day retrieval, $c\text{-}Fos^+$ cell density was greater in the upper than the lower blade, and there was a main effect of IEG (*p = 0.0236). **F** Mean $Arc^+c\text{-}Fos^+$ co-labeling normalized to chance (dotted line) was greater in the lower than upper blade during no shock, encoding, and 5-day retrieval. **G** Among complements of labeled DG cells, $Arc^+c\text{-}Fos^-$ cell density did not differ between blades but varied across memory states (main effect, *p = 0.0157). **H**, **I** $Arc^+c\text{-}Fos^+$ and $Arc^-c\text{-}Fos^+$ cell densities were greater in the upper than the lower blade during no shock, encoding, and 5-day retrieval. $Arc^+c\text{-}Fos^+$ cell density was greater in the upper than the lower blade at 1-day retrieval, and within the upper blade, greater during no shock than 1-day and 5-day retrieval. All labeled upper (**J**) and lower blade (**K**) cells for each group, summed across all mice, as a Venn diagram of Arc, c-Fos, and their overlap (blue) (upper: n = 1179, n = 3445, n = 3751, and n = 3871 cells; lower: n = 521, n = 1513, n = 1950, and n = 1953 cells). **L** The upper:lower density ratio was greater for c-Fos than Arc but not modulated by memory state. **M** This ratio for all labeled cells did not change across timepoints but was greater than 1 (dotted line) at each (one-sample *t*-tests, *p = 0.0375, ****p < 0.0001, ***p = 0.0002, and ***p = 0.0008). **N** Among complements, the $Arc^+c\text{-}Fos^-$ blade ratio was modulated by memory state, with that of encoding greater than that of all other groups, while both encoding and 1-day retrieval mean ratios were greater than 1 (one-sample *t*-tests, ***p = 0.0004, and **p = 0.0093). **O**, **P** $Arc^+c\text{-}Fos^+$ and $Arc^-c\text{-}Fos^+$ blade ratios were both greater than 1 at encoding and retrieval but not no shock timepoints (one-sample *t*-tests, ***p = 0.0005, **p = 0.0024, and ***p = 0.0009; **p = 0.0068, *p = 0.0129, and **p = 0.0024) but were not modulated by memory state. N = 4 (no shock) or 8 (encoding, 1-day retrieval, 5-day retrieval) mice. Error bars indicate ±SEM. *p < 0.05; **p < 0.01; ***p < 0.001; ****p < 0.0001. DG dentate gyrus, ∪ union.

Arc but not c-Fos expression varies by memory state and sub-region in the hippocampus

We first examined the expression of Arc and c-Fos across both upper and lower blades of the DG (Fig. 2A), given the region's essential role in memory encoding and retrieval[46] and the preferential recruitment of the upper blade across an array of behaviors[47]. In the DG, $c\text{-}Fos^+$ cells showed higher density in the upper than the lower blade across all memory states, while Arc^+ cells showed the same at no shock, encoding, and 5-day retrieval (Fig. 2B–E). However, across blades and timepoints, Arc^+ and $c\text{-}Fos^+$ cell density generally did not differ, with only a main effect of IEG at 1-day retrieval. As a measure of coordinated expression of both genes, their observed co-labeling was normalized to that expected if Arc^+ and $c\text{-}Fos^+$ cells were randomly distributed, and observed overlap was greatly above chance at all timepoints in both blades (Fig. 2F). Interestingly, this metric was greater in the lower than the upper blade at no shock, encoding, and 5-day retrieval timepoints, suggesting overall greater correspondence between Arc and c-Fos labeling in the lower blade. Cells were then further divided by blade into three complements based on their shared or unique expression: $Arc^+c\text{-}Fos^-$ cells (Fig. 2G), $Arc^+c\text{-}Fos^+$ cells (Fig. 2H), and $Arc^-c\text{-}Fos^+$ cells (Fig. 2I). Cells were quantified in all three complements across both blades and all timepoints, indicating that Arc and c-Fos expression patterns indeed diverged regardless of behavioral condition. While memory state had a main effect on cell density in the $Arc^+c\text{-}Fos^-$ complement, blade had an effect on $Arc^+c\text{-}Fos^+$ and $Arc^-c\text{-}Fos^+$ cell densities, with greater density in the upper blade than the lower in all conditions among $Arc^+c\text{-}Fos^+$ cells and in no shock, encoding, and 5-day retrieval among $Arc^-c\text{-}Fos^+$ cells. Furthermore, $Arc^+c\text{-}Fos^+$ cell density in the upper blade was greater in control no shock conditions than in both retrieval conditions, suggesting a subtle effect of memory state on co-expression of Arc and c-Fos in the DG. To better visualize these complements, Venn diagrams were generated of Arc^+ and $c\text{-}Fos^+$ cells summed across all sections, quantified for all mice in each group (Fig. 2J, K), highlighting substantial divergence in Arc and c-Fos expression despite a plurality of co-labeled cells. Such a divergence cannot be explained by the inability of cells to express one or the other IEG, as activation of the DG via administration of kainic acid induced both Arc and c-Fos expression in virtually every granule cell in both blades (Fig. S2).

Next, to better understand the relative expression of Arc and c-Fos between blades, the ratio of cell density in the upper to the lower blade was calculated per mouse. All calculated ratios at all timepoints were greater than 1, showing again that the upper blade displayed greater density of IEG labeling than the lower blade, and this ratio among $c\text{-}Fos^+$ cells was greater overall than that among Arc^+ cells (Fig. 2L). The mean upper:lower ratio for all labeled cells ($Arc^+ \cup c\text{-}Fos^+$) per group significantly exceeded 1 at every time point but was not influenced by memory state (Fig. 2M). Finally, among complement populations, this ratio was greater at encoding than at any other timepoint among $Arc^+c\text{-}Fos^-$ cells alone, with no effect of timepoint among $Arc^+c\text{-}Fos^+$ or $Arc^-c\text{-}Fos^+$ cells (Fig. 2N–P), indicating that the balance of cells expressing only Arc is biased toward the upper blade during CFC encoding specifically. Overall, these results provide evidence of substantial populations of active DG cells that express only Arc or c-Fos but not both, and they suggest that Arc and c-Fos expression are largely invariant to the memory state that induced them.

A more prominent effect of memory state, however, was found in CA3 (Fig. 3A). Arc^+ cell density increased from both no shock and encoding to 1-day retrieval and from encoding to 5-day retrieval (Fig. 3B), reflected in corresponding increases in $Arc^+c\text{-}Fos^-$ cell density from both no shock and encoding to both 1-day and 5-day retrieval, and in $Arc^+c\text{-}Fos^+$ cell density from encoding to 1-day and 5-day retrieval (Fig. 3C, D). These increases corresponded to commensurate decreases in $Arc^-c\text{-}Fos^+$ cell density from both no shock and encoding to 1-day retrieval and from encoding to 5-day retrieval (Fig. 3E), altogether suggesting that an increase in Arc across time occurs in $c\text{-}Fos^-$ and $c\text{-}Fos^+$ CA3 populations alike, despite total Arc or c-Fos labeling not changing over time (Fig. 3F). Nonetheless, $Arc^+c\text{-}Fos^+$ co-labeling occurred at levels greater than chance (Fig. 3G), suggesting that expression of the two IEGs was still generally coordinated in this region. Variations across memory states were also reflected in the fraction of labeled cells per complement at each timepoint (Fig. 3H–L), with the greatest proportion of CA3 cells $Arc^-c\text{-}Fos^+$, then $Arc^+c\text{-}Fos^+$, then $Arc^+c\text{-}Fos^-$ at no shock and encoding (Fig. 3H, I), a greater proportion $Arc^+c\text{-}Fos^+$ than $Arc^+c\text{-}Fos^-$ at 1-day retrieval (Fig. 3I), and a greater proportion $Arc^+c\text{-}Fos^+$ or $Arc^-c\text{-}Fos^+$ than $Arc^+c\text{-}Fos^-$ at 5-day retrieval (Fig. 3J). These data emphasize that memory state has a profound influence on IEG expression in CA3, identifying an increase in Arc expression from baseline and memory encoding to memory retrieval at multiple timepoints that appears independent of c-Fos expression.

In order to further confirm that divergence in Arc and c-Fos expression patterns in the HPC was not due to underlying cell type differences, we quantified expression of both IEGs in $GAD67^+$ inhibitory neurons in a subset of mice euthanized 1 h after 5-day CFC retrieval (Fig. S3A). As in the data above (Fig. 2E), DG Arc^+ and $c\text{-}Fos^+$ cell density did not differ (Fig. S3B), but a larger portion of $GAD67^+$ cells expressed c-Fos than Arc (Fig. S3C). Nonetheless, these $GAD67^+$ cells comprise only a fraction of the cells that express Arc or c-Fos alone (Fig. S3D). Overall CA3 $c\text{-}Fos^+$ cell density was greater than Arc^+ cell density (Fig. S3E), again aligning with findings above (Fig. 3B), and once again a greater portion of $GAD67^+$ cells expressed c-Fos than Arc (Fig. S3F). As in the DG, however, these $GAD67^+$ cells comprised a very small fraction of the cells that expressed either IEG alone (Fig. S3G), suggesting that differences in Arc and c-Fos labeling in the HPC cannot be explained by a difference in expression in underlying cell types, at least at a 5-day retrieval timepoint.

Arc and c-Fos expression patterns diverge in the basolateral amygdala complex, the ventral retrosplenial cortex, and the ventral anterior cingulate cortex

We next examined Arc and c-Fos expression in the BLA and RSCv, limbic brain regions both involved in fear memory, and the ACAv, a prefrontal cortical region thought to be involved in longer-term memory recall. In

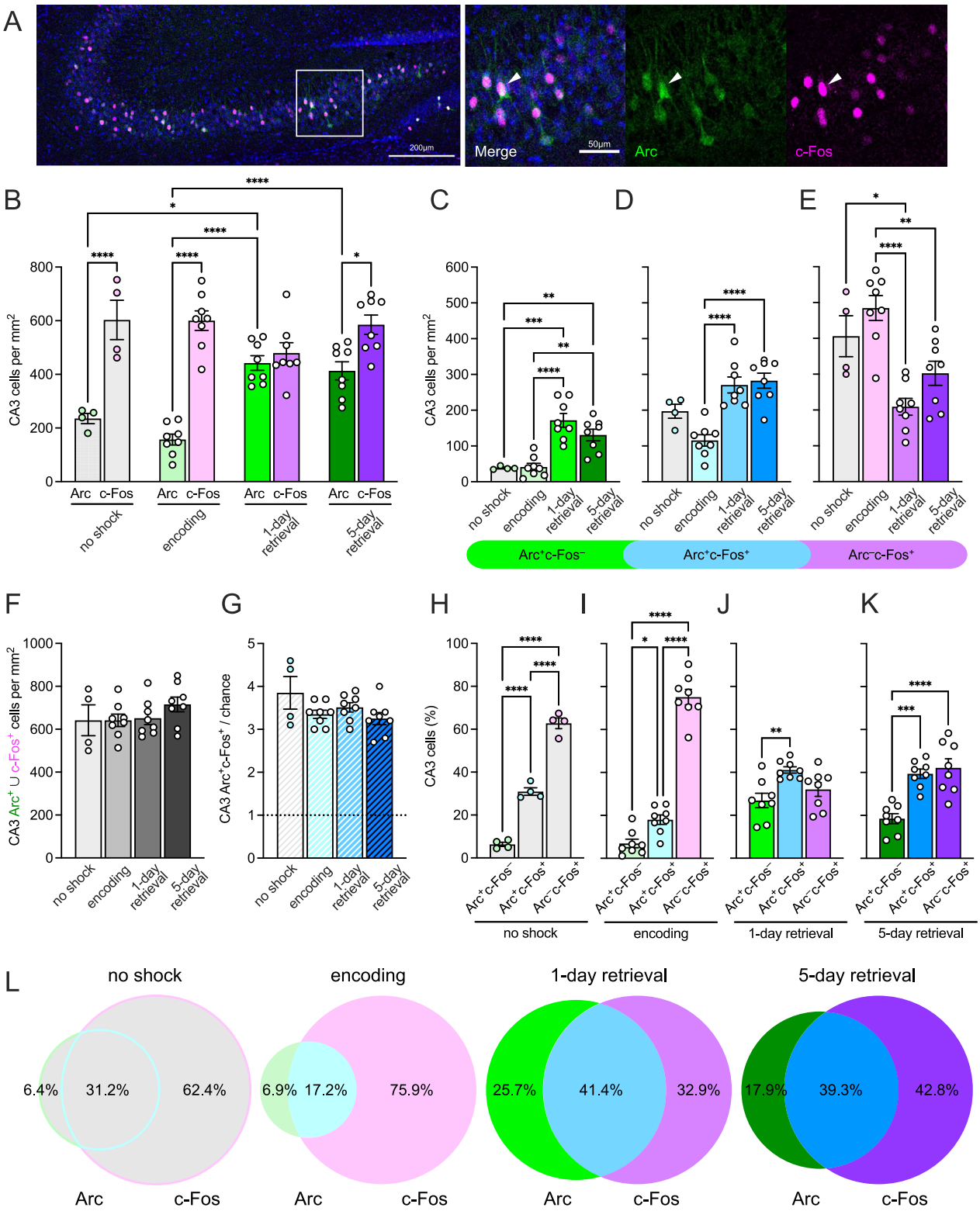

contrast to the DG but similar to CA3, BLA c-Fos$^+$ cell density was significantly greater than Arc$^+$ cell density at a no shock baseline and at CFC encoding (Fig. 4A, B). Though neither Arc$^+$ nor c-Fos$^+$ cell density varied across memory states, Arc$^+$c-Fos$^-$ cell density increased from no shock to 1-day retrieval, and Arc$^-$c-Fos$^+$ cell density decreased from encoding to 5-day retrieval (Fig. 4C–E), while overall expression remained constant (Fig. 4F). Arc$^+$c-Fos$^+$ co-labeling in the BLA was significantly greater than chance at all timepoints (Fig. 4G), and among complements, a greater proportion of cells were Arc$^-$c-Fos$^+$ than Arc$^+$c-Fos$^-$ at every timepoint and than Arc$^+$c-Fos$^+$ cells at no shock, encoding, and 5-day retrieval (Fig. 4H–L). Arc$^+$c-Fos$^+$ cell density was also greater than Arc$^+$c-Fos$^-$ cell density in no shock and encoding groups, collectively suggesting that Arc and c-Fos are expressed at different levels at both baseline and experimental behavioral conditions.

Fig. 3 | Arc but not c-Fos expression varies with memory state in CA3. A Left: representative section showing Arc (green) and c-Fos (magenta) expression with Hoechst nuclear counterstain (blue). Right: inset, with Arc and c-Fos channels presented separately. White arrow: example $Arc^+c\text{-}Fos^+$ cell. **B** Densities of Arc^+ and $c\text{-}Fos^+$ CA3 cells varied significantly by IEG and timepoint. In no shock, encoding, and 5-day retrieval groups, $c\text{-}Fos^+$ cell density was greater than Arc^+ cell density. Arc^+ cell density also increased from no shock to 1-day retrieval and from encoding to both 1-day and 5-day retrieval timepoints (significant interaction comparisons, not shown, are detailed in Supplementary Table 2). Among complements, **C** $Arc^+c\text{-}Fos^-$ cell density increased from both no shock and encoding to both 1-day and 5-day retrieval. **D** $Arc^+c\text{-}Fos^+$ cell density increased from encoding to both retrieval timepoints. **E** $Arc^-c\text{-}Fos^+$ cell density decreased from no shock to 1-day retrieval and from encoding to both retrieval timepoints. **F** There was no effect of timepoint on the density of the total number of CA3 cells expressing Arc or c-Fos. **G** The level of $Arc^+c\text{-}Fos^+$ co-labeling normalized to expected chance levels (dotted line) did not differ between timepoints, but at each timepoint mean co-labeling was greatly above chance (one-sample *t*-tests, $^{**}p = 0.0049$, $^{****}p < 0.0001$, $^{****}p < 0.0001$, $^{****}p < 0.0001$). Among complements of cells in the **H** no shock and **I** encoding groups, the $Arc^-c\text{-}Fos^+$ proportion was greater than both $Arc^+c\text{-}Fos^-$ and $Arc^+c\text{-}Fos^+$ proportions, while a greater proportion of cells were $Arc^+c\text{-}Fos^+$ than $Arc^+c\text{-}Fos^-$. **J** At 1-day retrieval, a greater proportion of cells were $Arc^+c\text{-}Fos^+$ than $Arc^+c\text{-}Fos^-$. **K** At 5-day retrieval, both the $Arc^+c\text{-}Fos^+$ and $Arc^-c\text{-}Fos^+$ proportions were greater than the $Arc^+c\text{-}Fos^-$ proportion. **L** All labeled CA3 cells for each group, summed across all sections quantified for all mice, represented as a Venn diagram of Arc expression (green), c-Fos expression (magenta), and their overlap (blue) (n = 2424, n = 5801, n = 6223, and n = 7415 cells, respectively). Percentages of total cells in each complement are overlaid for each timepoint. N = 4 (no shock) or 8 (encoding, 1-day retrieval, 5-day retrieval) mice. Error bars indicate ±SEM. $^*p < 0.05$; $^{**}p < 0.01$; $^{***}p < 0.001$; $^{****}p < 0.0001$. ∪ union.

The RSCv, considered part of the limbic memory circuit alongside the HPC and anterior thalamus[38], revealed subtle effects of memory state on IEG expression (Fig. 5A). First, in the no shock group, $c\text{-}Fos^+$ cell density was greater than Arc^+ cell density, but this difference was not detected in any CFC experimental group, and timepoint had no overall main effect (Fig. 5B). Next, while $Arc^+c\text{-}Fos^+$ cell density did not vary between memory states, $Arc^+c\text{-}Fos^-$ and $Arc^-c\text{-}Fos^+$ cell densities showed inverse parallel trends, with the former increasing from no shock to both encoding and 1-day retrieval conditions and the latter decreasing from both no shock and encoding to 1-day retrieval groups (Fig. 5C–E) while total labeled RSCv cell density remained constant (Fig. 5F). $Arc^+c\text{-}Fos^+$ co-labeling was above expected chance levels for all groups and varied with timepoint (main effect), though this metric did not differ between any two timepoints in individual comparisons (Fig. 5G). Finally, among complements of cells, at a no shock baseline the $Arc^-c\text{-}Fos^+$ proportion was greatest, followed by $Arc^+c\text{-}Fos^+$, and then $Arc^+c\text{-}Fos^-$, matching trends observed in several other brain regions assessed here (Fig. 5H). At encoding, a greater proportion of cells were $Arc^-c\text{-}Fos^+$ than either $Arc^+c\text{-}Fos^-$ or $Arc^+c\text{-}Fos^+$, and at 5-day retrieval, a greater proportion were either $Arc^+c\text{-}Fos^+$ or $Arc^-c\text{-}Fos^+$ than $Arc^+c\text{-}Fos^-$ (Fig. 5I–K), while all timepoints showed less than 40% co-labeling (Fig. 5L). These data show that Arc and c-Fos expression patterns diverge in the BLA and RSCv as in the HPC, and they suggest that memory state influences these patterns, though to a lesser degree than in CA3.

To compare these findings to another cortical region more typically associated with long-term memory retrieval, we also quantified IEG expression in the ACAv, a subregion of the dmPFC (Fig. S4A). Here, $c\text{-}Fos^+$ cell density was greater than Arc^+ cell density at each timepoint (Fig. S4B), but timepoint did not have any influence on either of these densities, the density of any complement of cells, or the density of Arc or c-Fos labeling overall (Fig. S4C–F). As in other regions, the rate of $Arc^+c\text{-}Fos^+$ co-labeling was above chance in all groups, indicating broad coordination in Arc and c-Fos expression, but this metric was not influenced by timepoint (Fig. S4G). Finally, within every timepoint, the $Arc^-c\text{-}Fos^+$ proportion of labeled cells exceeded both other complements, and the $Arc^+c\text{-}Fos^+$ proportion often exceeded the $Arc^+c\text{-}Fos^-$ proportion, again reflecting trends shown in other brain regions (Fig. S4H–L). Broadly, these data indicate that over a span of 5 days, encoding or retrieval of a CFC memory does not alter Arc or c-Fos expression in this subregion of the dmPFC from a no shock baseline. Compared to the effects observed in the RSCv, these findings thus suggest that IEG expression in different cortical areas may have different sensitivities to behavioral states.

c-Fos expression is greater than Arc expression at all memory states in the paraventricular nucleus of the thalamus and the lateral habenula

Finally, we examined two subcortical regions that are both involved in aspects of fear memory, the PVT and LH. Most remarkably, in the PVT, $c\text{-}Fos^+$ cell density was much greater than Arc^+ cell density at every memory state (Fig. 6A, B). Among complements, $Arc^+c\text{-}Fos^-$ cell density was greater in the encoding group than the no shock and 5-day retrieval groups, while $Arc^+c\text{-}Fos^+$ cell density was greater in the encoding group than the no shock group only (Fig. 6C, D). In contrast, $Arc^-c\text{-}Fos^+$ and total PVT labeled cell densities remained constant across timepoints (Fig. 6E, F). As in other regions, the level of normalized $Arc^+c\text{-}Fos^+$ co-labeling was above chance in every group, though interestingly, this rate decreased from no shock to all other memory states, representing a relative decorrelation of Arc and c-Fos expression with shock or shock memory retrieval (Fig. 6G). Nonetheless, a much greater proportion of cells were $Arc^-c\text{-}Fos^+$ than both other complements at every memory state (Fig. 6H–K), composing 90–95% of all cells labeled in the PVT (Fig. 6L).

Finally, in the LH, $c\text{-}Fos^+$ cell density was greater than Arc^+ cell density at each timepoint and greater at 5-day than 1-day retrieval (Fig. 7A, B). Among complements, $Arc^+c\text{-}Fos^-$ cell density was greater at encoding than at a no shock baseline, and $Arc^+c\text{-}Fos^+$ cell density was greater at 5-day retrieval than at a no shock baseline (Fig. 7C–E). Interestingly, the LH showed a decrease in total labeled cell density from CFC encoding to 1-day retrieval (Fig. 7F), which may correspond to changing stress levels across exposures to the conditioned context[48]. All rates of co-labeling normalized to chance were once again greater than 1, though as in the PVT, this metric decreased from the no shock group to the encoding and 5-day retrieval groups, again representing a decorrelation of IEG expression at these latter timepoints (Fig. 7G). In the LH, at every timepoint, the $Arc^-c\text{-}Fos^+$ proportion of cells was significantly greater than both other complements in all groups (Fig. 7H–K), with the Arc^+ and $c\text{-}Fos^+$ populations sharing a maximum of 12.5% overlap among all quantified LH cells (Fig. 7L). In sum, though both the PVT and LH displayed profound differences in expression of Arc and c-Fos, memory state only subtly impacted IEG expression in these regions overall.

Discussion

In this study, we cataloged the simultaneous expression of the IEGs Arc and c-Fos in seven regions of the mouse brain at four timepoints: during novel context (no shock) exposure, during encoding of a CFC memory, during retrieval of that memory 1 day later, or during retrieval 5 days later. We showed that expression differed greatly between Arc and c-Fos, with substantial numbers of cells in every brain region across all timepoints positive for Arc or c-Fos but not both. In the DG, Arc and c-Fos expression did not vary or varied only subtly with memory state, in contrast to CA3 where Arc but not c-Fos expression increased substantially from CFC encoding to retrieval. In the BLA and RSCv, but not the ACAv, memory state influenced some aspects of the relative expression of Arc and c-Fos, and in the subcortical regions PVT and LH, expression of c-Fos vastly exceeded that of Arc across all memory states. Though patterns of Arc and c-Fos expression were not independent of one another, as evidenced by their rate of co-labeling above chance in every region examined, these data strongly suggest that factors beyond neuronal activity alone determine whether Arc and c-Fos are expressed.

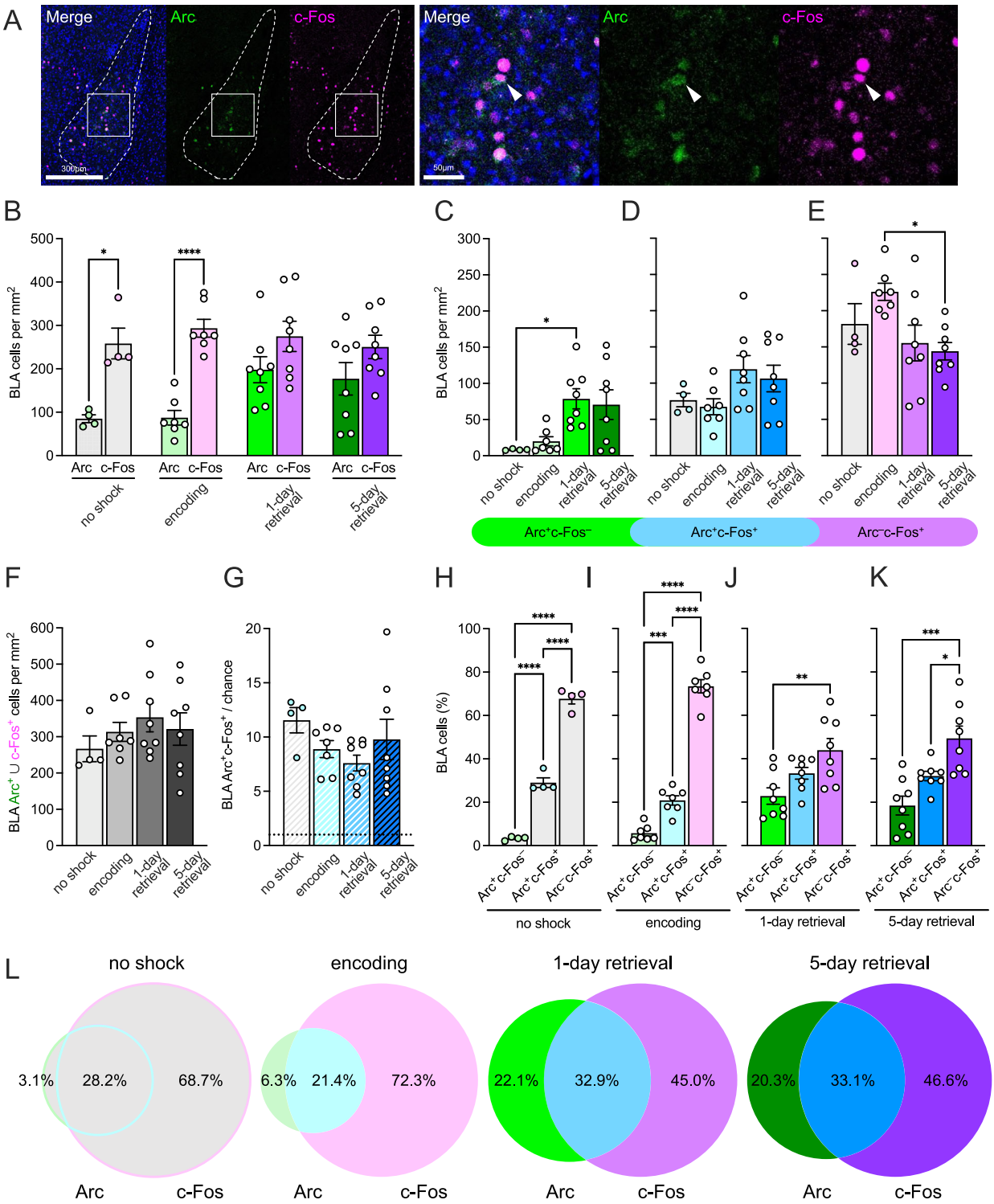

Fig. 4 | Arc and c-Fos expression differ in the BLA but are not strongly influenced by memory state. A Left: representative section (BLA in dotted outline) showing Arc (green) and c-Fos (magenta) expression with a Hoechst nuclear counterstain (blue). Right: inset, with Arc and c-Fos channels presented separately. White arrow: example $Arc^+c\text{-}Fos^+$ cell. **B** $c\text{-}Fos^+$ cell density was greater than Arc^+ cell density in the no shock and encoding groups. **C** $Arc^+c\text{-}Fos^-$ cell density increased from no shock to 1-day retrieval. While **D** $Arc^+c\text{-}Fos^+$ cell density did not change with memory state, **E** $Arc^-c\text{-}Fos^+$ cell density decreased from encoding to 5-day retrieval. **F** The density of the total number of BLA cells expressing Arc or c-Fos did not differ across timepoints. **G** The level of $Arc^+c\text{-}Fos^+$ co-labeling normalized to expected chance levels (dotted line) did not differ between timepoints, but at each timepoint mean co-labeling was above chance (one-sample *t*-tests, $^{**}p = 0.0029$, $^{****}p < 0.0001$, $^{****}p < 0.0001$, and $^{**}p = 0.0021$ respectively). Among complements of all cells in **H** no shock and **I** encoding groups, the greatest proportion of cells were $Arc^-c\text{-}Fos^+$, followed by $Arc^+c\text{-}Fos^+$, then $Arc^+c\text{-}Fos^-$. **J** At 1-day retrieval, a greater proportion of cells were $Arc^-c\text{-}Fos^+$ than $Arc^+c\text{-}Fos^-$. **K** At 5-day retrieval, a greater proportion of cells were $Arc^-c\text{-}Fos^+$ than $Arc^+c\text{-}Fos^-$ or $Arc^+c\text{-}Fos^+$. **L** All labeled BLA cells for each group, summed across all sections quantified for all mice, represented as a Venn diagram of Arc expression (green), c-Fos expression (magenta), and their overlap (blue) (n = 2654, n = 4439, n = 6080, and n = 5248 cells, respectively). Percentages of total cells in each complement are overlaid for each timepoint. N = 4 (no shock), 7 (encoding), or 8 (1-day retrieval, 5-day retrieval) mice. Error bars indicate ±SEM. $^*p < 0.05$; $^{**}p < 0.01$; $^{***}p < 0.001$; $^{****}p < 0.0001$. BLA basolateral amygdala complex, ∪ union.

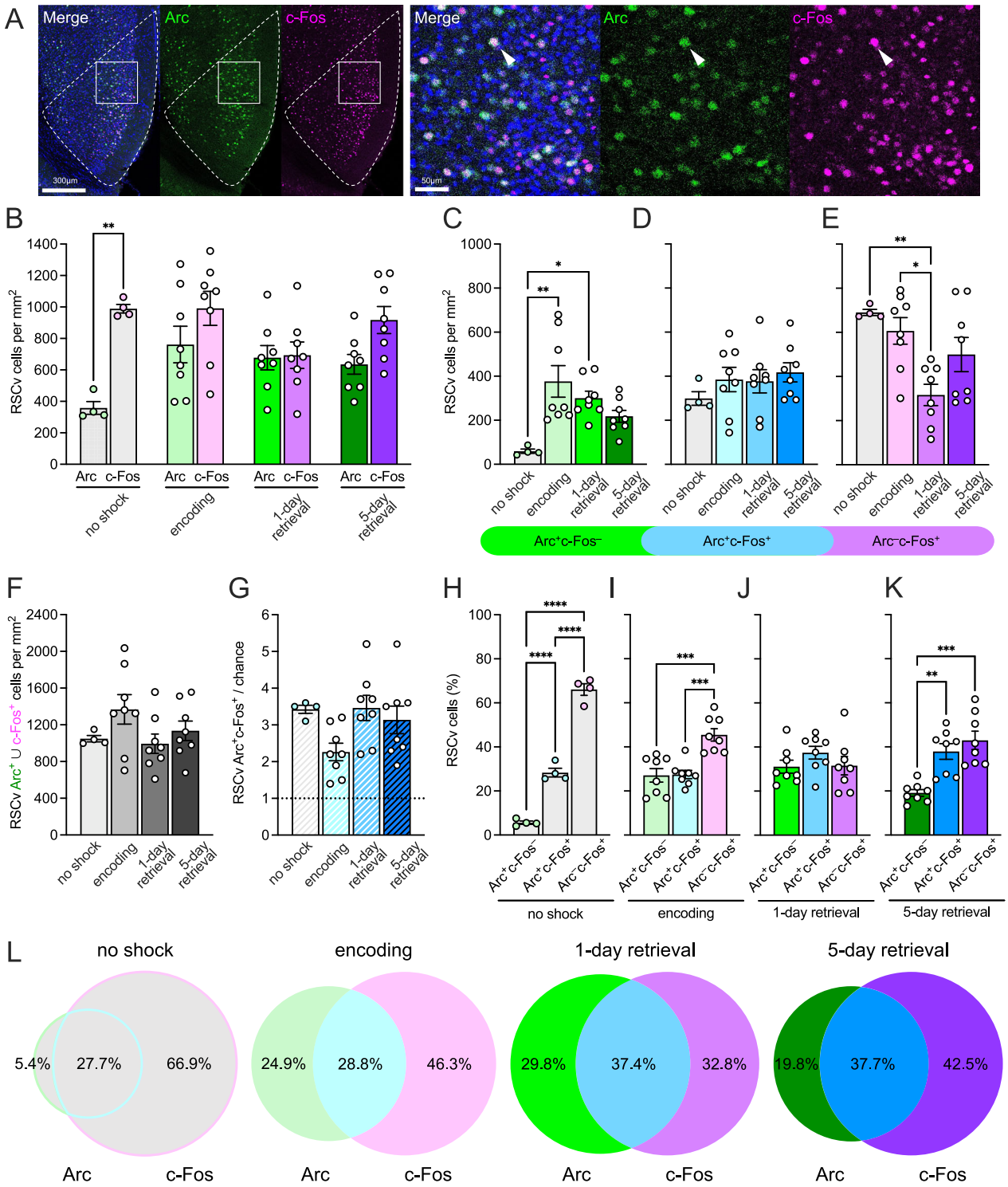

One variable influencing IEG expression is the different molecular and electrophysiological conditions under which these genes are transcribed and translated[49]. *c-Fos* mRNA in the DG, for example, does not correlate with burst firing observed in field recordings during electrically-induced seizures in rats[50], decoupling its expression from neuronal activity. One possible cause of this discrepancy is ΔFosB, a TF that represses c-Fos and is upregulated in phenomena as varied as cocaine administration[51], repeated training in a spatial task[52], and spontaneous seizures in Alzheimer's disease (AD) and epilepsy model mice[53]. Conversely, Arc induces repeated cycles of its own transcription following stimulation[20] and is expressed differentially between cells of the same type in different brain regions[31], identifying characteristics of Arc that likewise separate its expression from direct neural firing. The expression of both genes is also induced by distinct sets of enhancers activated in stimulus-specific manners[54], adding an additional epigenetic regulatory layer that may result in expression of Arc or c-Fos but not both. Furthermore, we found here that c-Fos was more highly expressed than Arc in GAD67$^+$ hippocampal interneurons, and while this discrepancy only explained a small fraction of the divergence of the two genes, other brain regions may have greater proportions of inhibitory neurons that bias their overall expression toward c-Fos. Lastly, both c-Fos and Arc have been

Fig. 5 | Arc and c-Fos expression patterns diverge in the RSCv at all memory states. A Left: representative section (RSCv in dotted outline) showing Arc (green) and c-Fos (magenta) expression with a Hoechst nuclear counterstain (blue). Right: inset, with Arc and c-Fos channels presented separately. White arrow: example $Arc^+c\text{-}Fos^+$ cell. **B** RSCv $c\text{-}Fos^+$ cell density was greater than that of Arc^+ cells in the no shock control group (significant interaction comparisons, not shown, are detailed in Supplementary Table 2). **C** $Arc^+c\text{-}Fos^-$ cell density increased from no shock to both encoding and 1-day retrieval timepoints. **D** $Arc^+c\text{-}Fos^+$ cell density did not significantly differ across timepoints. **E** $Arc^-c\text{-}Fos^+$ cell density decreased from both no shock and encoding groups to 1-day retrieval. **F** There was no effect of timepoint on the density of the total number of RSCv cells expressing Arc or c-Fos. **G** The level of $Arc^+c\text{-}Fos^+$ co-labeling normalized to expected chance levels (dotted line) differed with timepoint (main effect, $^*p = 0.0449$) but not between timepoints in post hoc comparisons. At each timepoint, mean co-labeling was above chance (one-sample *t*-tests, $^{***}p = 0.0002$, $^{**}p = 0.0011$, $^{***}p = 0.0002$, and $^{***}p = 0.0007$ respectively). **H** Among complements of all labeled cells in the no shock group, a greater proportion were $Arc^-c\text{-}Fos^+$ than $Arc^+c\text{-}Fos^-$ or $Arc^+c\text{-}Fos^+$, and a greater proportion were $Arc^+c\text{-}Fos^+$ than $Arc^+c\text{-}Fos^-$. **I** At encoding, a greater proportion were $Arc^-c\text{-}Fos^+$ than either $Arc^+c\text{-}Fos^-$ or $Arc^+c\text{-}Fos^+$. While complement proportions did not differ at **J** 1-day retrieval, **K** both $Arc^+c\text{-}Fos^+$ and $Arc^-c\text{-}Fos^+$ proportions were greater than the $Arc^+c\text{-}Fos^-$ proportion at 5-day retrieval. **L** All labeled RSCv cells for each group, summed across all sections quantified for all mice, represented as a Venn diagram of Arc expression (green), c-Fos expression (magenta), and their overlap (blue) (n = 11,472, n = 30,984, n = 27,188, and n = 27,263 cells, respectively). Percentages of total cells in each complement are overlaid for each timepoint. N = 4 (no shock) or 8 (encoding, 1-day retrieval, 5-day retrieval) mice. Error bars indicate ±SEM. $^*p < 0.05$; $^{**}p < 0.01$; $^{***}p < 0.001$; $^{****}p < 0.0001$. RSCv ventral retrosplenial cortex, ∪ union.

observed in glial cells[55,56], which may contribute to quantifications of IEG expression despite their dissociation from neurons entirely. Indeed, a recent study identified c-Fos-expressing astrocyte ensembles during learning whose activation could causally influence memory recall[57]. All together, these findings emphasize the many mechanisms that decorrelate the presence of c-Fos and Arc from one another and from neuronal activity or inactivity, possibly driving the divergence in their expression revealed here.

Past attempts at quantifying simultaneous Arc and c-Fos expression have been limited by their study of select brain regions or controlled cell culture conditions. In the DG, Stone et al. euthanized mice 1.5 h following testing of a water maze task and found 78.8% co-labeling among all Arc^+ or $c\text{-}Fos^+$ granule cells across mice[58]. Additionally, Rao-Ruiz et al. euthanized mice 1.5 h following context exposure and found 82.6% co-labeling among all Arc^+ or $c\text{-}Fos^+$ DG granule cells[59]. Possible reasons for the discrepancies between these studies and our data include different times elapsed before euthanasia, varying cognitive demands of the behavioral paradigms used, contrasting strategies for cell quantification, or nonspecific binding of host antibodies that match the same species as the tissue examined. Here, we did not use mouse antibodies, which historically have increased leak in mouse sections, but instead used rat and rabbit hosts and confirmed minimal leak with control experiments. Better aligning with our work, a recent study found that LTP in hippocampal cell cultures yielded only 53.1% co-labeling among all cells Arc^+ or $c\text{-}Fos^+$ on average[60], while another similarly found no more than 50% co-labeling in the hippocampus and amygdala after context exposure or fear conditioning. This latter study also did not detect Arc expression in the PVT or LH despite robust c-Fos detection, aligning with the present findings showing strong dominance of c-Fos in these regions[61]. Our work thus joins a growing body of evidence[62] that divergence in Arc, c-Fos, and other IEG expression is a robust brain-wide yet region-specific phenomenon occurring in various paradigms of neuronal activation.

This evidence that active sets of neurons have different IEG profiles also supports the perspective that a single engram is composed of multiple heterogeneous subunits[49,63–65]. Recent work has shown that DG ensembles tagged by c-Fos expression receive enhanced excitatory inputs and promote memory generalization, while those tagged by expression of another IEG, Npas4, receive enhanced inhibitory inputs and promote memory discrimination[66]. Separate gene regulatory mechanisms may underlie such functionally distinct ensembles, and neurons expressing Arc alone may constitute yet another of these units. To this end, using the expression of a full suite of IEGs to generate a multidimensional neuronal activation signature, as has been implemented for single-cell and spatial transcriptomics[67] and across various HPC cell types[68], may be especially critical in identifying active neurons in distinct subunits. Such an approach would also inform novel strategies to label and manipulate ensembles that express multiple IEGs, enabling increased control over the heterogeneous components that constitute an engram. Lastly, these subunits may even be leveraged to form a combinatorial decoder of brain state[69], where the expression patterns of multiple IEGs are together better at distinguishing one state from another than any IEG alone, or had all IEGs been expressed identically.

Finally, our results also suggest that Arc may be more dynamically responsive to memory state than c-Fos, particularly in areas like CA3 and RSCv. Indeed, some of the earliest work on expression of IEGs in the rat HPC found that levels of *Arc* but not *c-Fos* mRNA correlated with the strength of a spatial memory 0.5 h after its retrieval[16]. In this case, what role might an increase in Arc expression play in retrieval of a contextual fear memory compared to its encoding? Given its many functions in the cell, Arc may support memory strength in ways not directly corresponding to neuronal activity. For instance, one proposed function of Arc is homeostatic scaling via AMPAR endocytosis, where the strengths of all synapses of a neuron are scaled down while retaining their relative strengths to preserve the capacity for further potentiation[21,70]. Such a function may be more important for a highly recurrent region like CA3 than for a sparsely active region like the DG[71], and it may be more necessary during memory retrieval than encoding due to the role of CA3 in pattern completion. As CA3 ensembles reinstate a full representation of the encoded conditioning, Arc expression may be induced to maintain the specificity of the representation and prevent over-generalization, as homeostatic scaling has been shown to do in other brain regions like the gustatory cortex[72]. Alternatively, early lesion studies demonstrated that severing direct input to CA3 along the perforant path impaired retrieval but not encoding of a spatial navigation task[73], and it is possible that increased Arc^+ cell density specifically identifies CA3 cells newly recruited by direct input at memory retrieval. In either case, further research is needed to determine whether Arc in CA3 serves the same or a different role as in other brain areas such as the DG or BLA.

In summary, we found that two commonly used IEGs, Arc and c-Fos, showed divergent expression patterns across several brain regions and behavioral conditions in male mice. Arc in particular showed memory state dependence in regions such as hippocampal CA3, suggesting that engrams identified by its use may capture cells uniquely involved in memory processing. Conversely, the relative invariance of c-Fos expression between behavioral contexts and anatomical regions may encourage its use as a less biased proxy for neural activation across a wider array of behavioral phenomena. Importantly, future research is also needed to determine whether these findings are replicated in female mice, given the extensive literature revealing sex differences in IEG expression across behavioral tasks in several rodent and avian species[74–79]. With distinct molecular and regulatory features, it is not surprising that neither Arc nor c-Fos represents a complete portrait of all active cells, but the specific ways in which their expressions diverge should critically inform the way they are used to connect complex behaviors with the cell ensembles underlying them.

Methods

Mice

Male mice on a 129S6/SvEv background were generated in-house and used at 3 to 6 months of age. Mice were housed 4 to 5 per cage in a 12-h (06:00–18:00) light-dark colony room at 22 °C. Food and water were provided ad libitum.

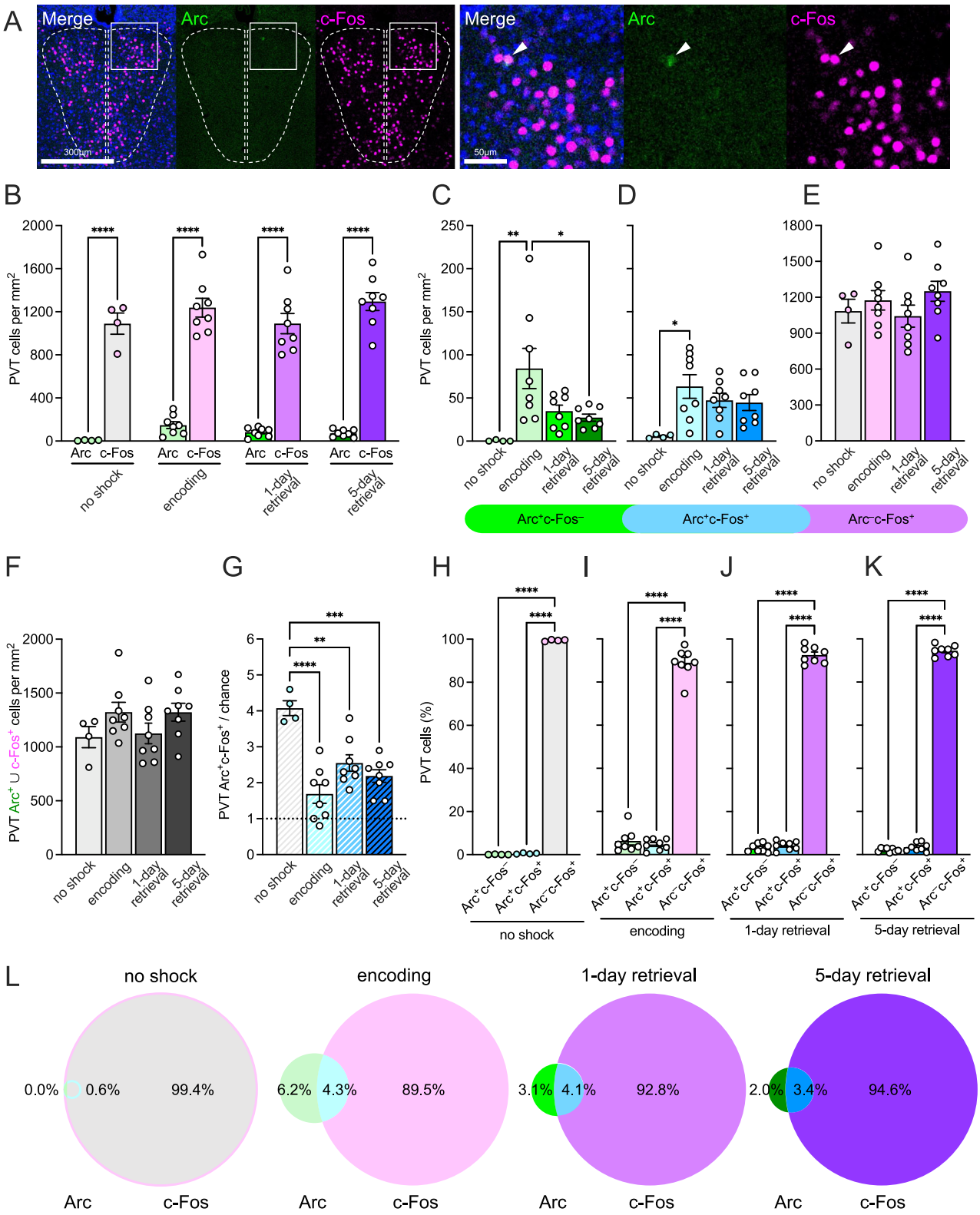

Behavioral testing was performed during the light phase. Some unavoidable but temporary discomfort (e.g., foot shock) was associated with testing. As a humane endpoint, if any mice displayed prolonged pain or distress, as evidenced by significant weight loss, signs of dehydration, poor grooming, signs of pain, and/or hunched posture due to unpredicted illness or injury, they would have been euthanized; however, no such unexpected adverse events occurred. We ensured that discomfort to the mice was limited to all possible extent while still completing the aims of this research. All experiments were approved by the Institutional Animal Care and Use Committees (IACUCs) at Columbia University Irving Medical Center (CUIMC) and the New York State Psychiatric Institute (NYSPI), and we have complied with all relevant ethical regulations for animal use.

Fig. 6 | c-Fos expression is greater than Arc expression and is independent of memory state in the PVT. A Left: representative section (PVT in dotted outline) showing Arc (green) and c-Fos (magenta) expression with a Hoechst nuclear counterstain (blue). Right: inset, with Arc and c-Fos channels presented separately. White arrow: example $Arc^+c\text{-}Fos^+$ cell. **B** PVT $c\text{-}Fos^+$ cell density was greater than that of Arc at every timepoint. **C** $Arc^+c\text{-}Fos^-$ cell density increased from no shock to encoding but decreased from encoding to 5-day retrieval. **D** $Arc^+c\text{-}Fos^+$ cell density increased only from the no shock to the encoding group. **E** $Arc^-c\text{-}Fos^+$ cell density did not differ across timepoints. **F** The density of the total number of PVT cells expressing Arc or c-Fos did not differ across timepoints. **G** The level of $Arc^+c\text{-}Fos^+$ co-labeling normalized to expected chance levels (dotted line) decreased from the no shock control group to every experimental timepoint. At each timepoint, mean co-labeling was above chance (one-sample *t*-tests, ***p = 0.0006, *p = 0.0323, ***p = 0.0003, and ***p = 0.0003 respectively). **H–K** Among complements of all labeled PVT cells, a greater proportion were $Arc^-c\text{-}Fos^+$ than $Arc^+c\text{-}Fos^-$ and than $Arc^+c\text{-}Fos^+$ at every timepoint. **L** All labeled PVT cells for each group, summed across all sections quantified for all mice, represented as a Venn diagram of Arc expression (green), c-Fos expression (magenta), and their overlap (blue) (n = 2494, n = 5977, n = 5075, and n = 6239 cells, respectively). Percentages of total cells in each complement are overlaid for each timepoint. N = 4 (no shock) or 8 (encoding, 1-day retrieval, 5-day retrieval) mice. Error bars indicate ±SEM. *p < 0.05; **p < 0.01; ***p < 0.001; ****p < 0.0001. PVT paraventricular nucleus of the thalamus, ∪ union.

Contextual fear conditioning (CFC)

A 3-shock CFC paradigm was administered as previously described[10]. Chambers with Plexiglas walls and a stainless-steel grid floor were obtained from Med Associates (St. Albans, VT). A house light (CM1820 bulb, 28 v, 100 mA) mounted directly above the chamber provided illumination. Each chamber was located inside a larger light- and sound-insulated plastic cabinet with a ventilation fan that operated during all behavior sessions. During both conditioning and context re-exposure, a paper towel dabbed with lemon scent was placed underneath the chamber floor. Mice were held outside the experimental room in their home cages prior to testing and transported to the conditioning apparatus individually in standard mouse cages. Chambers were cleaned with Virkon S (LANXESS, Cologne, Germany) before and after trials.

During conditioning trials, mice were placed into the chamber and received 2-s foot shocks of 0.75 mA at 180 s, 240 s, and 300 s after the start of the trial. Mice were removed from the chambers 15 s after termination of the final shock and returned to their home cage. During context re-exposure trials, the testing procedure and context was identical, except mice were placed in the conditioning chamber for 300 s and did not receive any foot shocks. All sessions were recorded with ceiling-mounted digital video cameras and freezing behavior in the first 180 s of each trial was scored using FreezeFrame software (v4, Actimetrics, Wilmette, IL). No criteria were set to exclude animals during the experiment. Regression analyses were run to assess whether freezing levels at retrieval in 1-day and 5-day groups correlated with IEG expression in any of the quantified regions, though no relationships were statistically significant.

Drugs

Kainic acid: Activation of the limbic system was induced via a single intraperitoneal (i.p.) injection of kainic acid in physiological saline (0.9% NaCl) at 20 mg per kg body weight[80]. This administration induced acute convulsive seizures that persisted for several minutes.

Immunohistochemistry

One hour after behavior, mice were anesthetized, and brains were extracted via transcardial perfusion. Brains were stored in 4% paraformaldehyde (PFA) in 1× phosphate buffered saline (PBS) overnight, then in 1× PBS. Brains were sectioned at 40 µm thickness on a vibratome (Leica Biosystems, Wetzlar, Germany) and stored in 1× PBS with 0.1% sodium azide. Floating sections were used for all immunohistochemistry.

For Arc and c-Fos detection, sections were first washed 3 times in 1× PBS for 10 min each then blocked in 1× PBS with 0.5% Triton X-100 and 10% normal donkey serum (NDS) for 2 h at room temperature (RT). Incubation with primary antibodies (rat anti-c-Fos, 226 017, 1:5000; rabbit anti-Arc, 156 003, 1:1000; Synaptic Systems, Göttingen, Germany) in 1× PBS with 0.5% Triton X-100 was performed at 4 °C overnight. After primary incubation, sections were washed 3 times in 1× PBS for 10 min each and incubated in secondary antibodies (donkey anti-rat Alexa Fluor 647, ab150155, 1:500; donkey anti-rabbit Alexa Fluor 488, ab150073, 1:500; Abcam, Cambridge, UK) in 1× PBS for 2 h at RT. After secondary incubation, sections were washed 3 times in 1× PBS for 10 min each then counterstained with Hoechst 33342 (1:10,000, Thermo Fisher Scientific, Waltham, MA) in 1× PBS for 15 min at RT. Sections were washed in 1× PBS for 10 min then mounted on slides before adding mounting medium Fluoromount-G (Southern Biotechnology Associates, Inc., Birmingham, AL) and a coverslip approximately 30 min later.

For GAD67 detection alongside Arc and c-Fos, the protocol above was modified to use a 30 min permeabilization in 1× PBS with 0.1% Triton X-100 at RT, the addition of a blocking step for 1 h in 1× PBS with 5% NDS and 3% bovine serum albumin (BSA) at RT, and a 48 h incubation in primary antibodies in this blocking buffer, adding mouse anti-GAD67 (MAB5406, Sigma-Aldrich, Burlington, MA) at 1:500. Secondary incubation also occurred in blocking buffer, with the addition of donkey anti-mouse Cy3 (715-165-150, Jackson ImmunoResearch, West Grove, PA) at 1:250.

Prior to determining the combination of Arc and c-Fos primary and secondary antibodies listed above, several other antibodies were tested to simultaneously detect IEG expression, as depicted in Supplementary Fig. 1 and described in Supplementary Table 1. In each of these tests, incubation lengths and temperatures were identical to above unless otherwise noted. In tests using AffiniPure Fab fragments (Jackson ImmunoResearch, West Grove, PA) to block extraneous antibody binding to mouse immunoglobulins, sections were incubated in a 0.1 mg per mL solution in 1× PBS with 0.5% Triton X-100 for 2 h at RT immediately prior to primary antibody incubation. In tests using a hydrochloric acid solution (pH = 1) for antigen retrieval, sections were incubated for 15 min at RT after initial washes then washed in 1× PBS for 10 min prior to NDS block. In tests using a sodium citrate solution (pH = 8.5) for antigen retrieval, sections were incubated for 1 h at 80 °C after initial washes then washed in 1× PBS for 10 min prior to NDS block. Finally, to ensure specificity of the antibodies chosen for use, control immunostains were run lacking either rat anti-c-Fos primary or rabbit anti-Arc primary but including both anti-rat and anti-rabbit secondary antibodies. These tests confirmed minimal cross-reactivity between Arc and c-Fos labels in the strategy detailed above.

Confocal microscopy and quantification

For Arc and c-Fos detection, all samples were imaged on a Leica TCS SP8 confocal scanning microscope with LAS X software (Leica Microsystems Inc., Wetzlar, Germany) and 2 simultaneous PMT detectors as previously described[81]. Images were taken in sequence, first with Alexa Fluor 488 excited at 488 nm and detected at 506–556 nm and Alexa Fluor 647 excited at 638 nm and detected at 646–696 nm. Then Hoechst 33342 was excited with ultraviolet light at 405 nm and detected at 429–478 nm. Laser power was held constant between all sections. Sections were imaged with a dry Leica 20x objective (NA 0.70, WD 0.5 mm) at a resolution of 1024 × 1024 and pixel size of 1.08 μm^2. Fields of view were stitched to form tiled images using an automated stage and the LAS X statistical blending algorithm with multi-frame search. Lastly, background fluorescence was subtracted from all images in Fiji (ImageJ) software (v2.16.0) prior to quantification[82].

To image GAD67 expression alongside Arc and c-Fos, excitation of Cy3 at 552 nm and detection at 543–593 nm was added simultaneous to Hoechst 33342 detection, and sections were imaged in a z-stack of 4 × 3 µm steps (9 µm depth total) to better capture limited numbers of $GAD67^+$ cells. Quantification as described below occurred in maximum projections of signal through this stack, with verification of colocalization within each slice as needed.

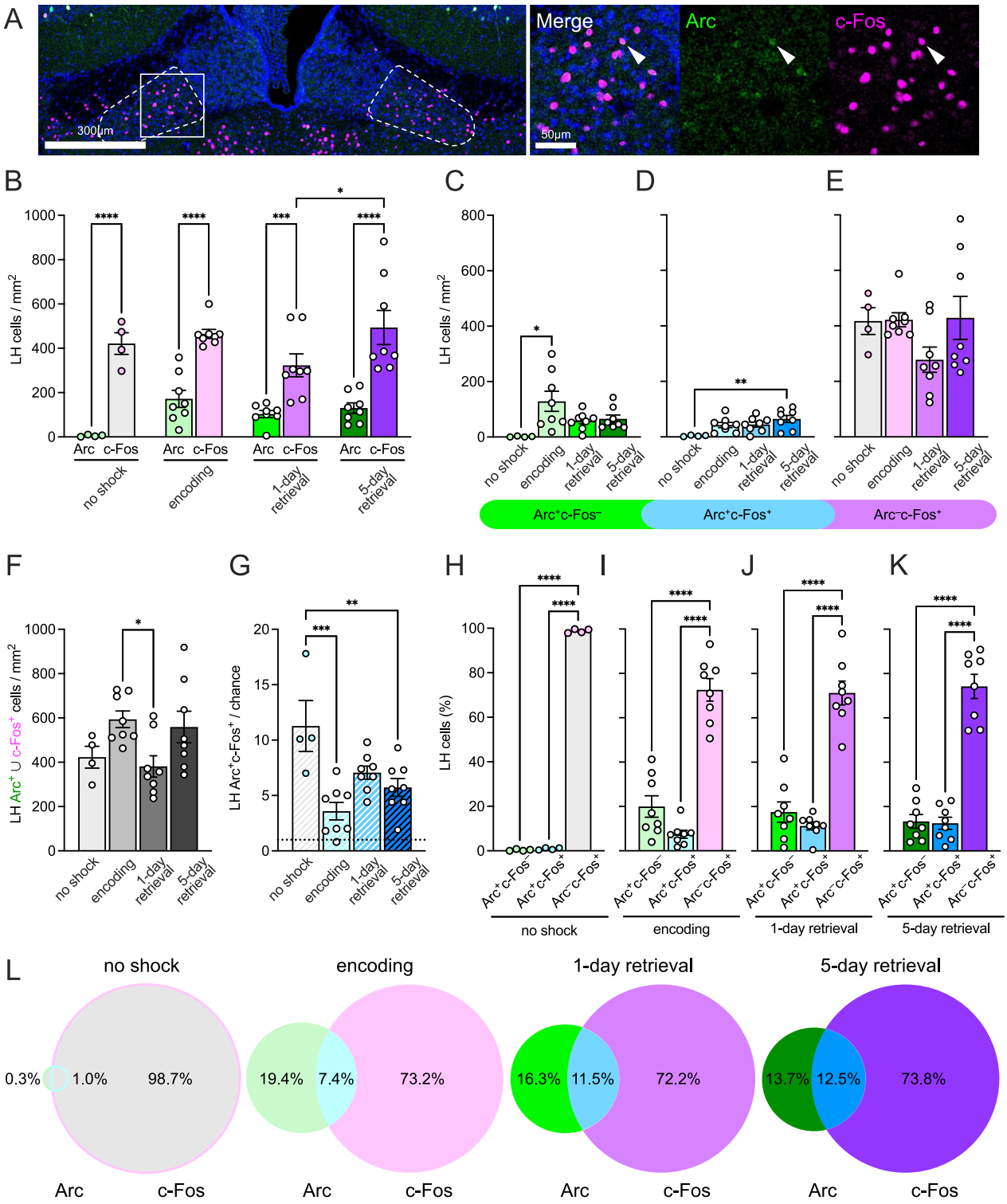

To assess expression of Arc and c-Fos in an unbiased manner, brain regions were first outlined using the polygon selection tool in the Hoechst channel of each image. Next, Arc and c-Fos channels were quantified individually, recording positive cells with the multi-point selection tool and storing the set as a region of interest (ROI) object for each respective marker. Then, to identify Arc$^+$c-Fos$^+$ cells, both ROI objects were overlaid on a merged-channel section image, and co-labeled cells were noted as those marked positive for each IEG separately. This set was marked and stored as a third and final ROI object. Data per mouse were summed from 3 to 4 bilateral sections (1 to 2 sections for the ACAv) and divided by total area quantified. BLA counts for one animal and ACAv counts for four animals were excluded for not meeting a threshold of 3 or 1 high-quality bilateral BLA or ACAv section(s) respectively. To calculate percentages of labeled cells by region, estimates of cells per mm^2 (per mm^3 for Arc/c-Fos/GAD67 counts) were generated by counting Hoechst$^+$ cells in 4 sections from each of 4 randomly selected experimental mice and averaging density across all mice by region. In dense regions like the DG, confocal images were taken with an oil-immersion Leica 63x

Fig. 7 | Arc and c-Fos expression patterns diverge in the LH across all memory states. A Left: representative section (LH in dotted outline) showing Arc (green) and c-Fos (magenta) expression with a Hoechst nuclear counterstain (blue). Right: inset, with Arc and c-Fos channels presented separately. White arrow: example $Arc^+c\text{-}Fos^+$ cell. **B** LH c-Fos^+ cell density was greater than that of Arc at every timepoint. c-Fos^+ cell density was also greater at 5-day than 1-day retrieval. Among complements of cells, **C** $Arc^+c\text{-}Fos^-$ cell density increased only from no shock to encoding timepoints, while **D** $Arc^+c\text{-}Fos^+$ cell density increased only from no shock to 5-day retrieval timepoints. **E** There was no difference in the density of $Arc^-c\text{-}Fos^+$ cells in the LH across timepoints. **F** Total LH Arc^+ or c-Fos^+ cell density decreased from CFC encoding to 1-day retrieval but did not differ from either timepoint to no shock or 5-day retrieval. **G** The level of $Arc^+c\text{-}Fos^+$ co-labeling normalized to expected chance levels (dotted line) decreased from no shock to both encoding and 5-day retrieval. At each timepoint, mean co-labeling was above chance (one-sample *t*-tests, *p = 0.0209, * p = 0.0135, ****p < 0.0001, and ***p = 0.0006 respectively). **H–K** Among complements of all labeled LH cells, a greater proportion were $Arc^-c\text{-}Fos^+$ than $Arc^+c\text{-}Fos^-$ and than $Arc^+c\text{-}Fos^+$ at every memory state. **K** All labeled LH cells for each group, summed across all sections quantified for all mice, represented as a Venn diagram of Arc expression (green), c-Fos expression (magenta), and their overlap (blue) (n = 1444, n = 1974, n = 1627, and n = 1857 cells, respectively). Percentages of total cells in each complement are overlaid for each timepoint. N = 4 (no shock) or 8 (encoding, 1-day retrieval, 5-day retrieval) mice. Error bars indicate ±SEM. *p < 0.05; **p < 0.01; ***p < 0.001; ****p < 0.0001. LH lateral habenula, ∪ union.

objective (NA 1.4, WD 0.14 mm), to aid in discriminating $Hoechst^+$ nuclei for quantification.

Statistics and reproducibility

All data were analyzed using Prism (v10.5.0, GraphPad, San Diego, CA) with alpha set to 0.05 and tests two-tailed where applicable. Results from analyses are expressed as means ± SEM. *p < 0.05, **p < 0.01, ***p < 0.001, ****p < 0.0001. Effects of blade, IEG, timepoint, and factor interactions were analyzed using one- or two-way analysis of variance (ANOVA) tests, where significant main effects were followed by Šídák's post-hoc comparisons within groups across the significant factor(s), adjusted for multiple comparisons. In two-way ANOVAs, comparisons between groups differing across both factors were only made following significant interaction effects. To test whether levels of $Arc^+c\text{-}Fos^+$ co-labeling were different from those expected by chance, a normalized value was calculated for each mouse using the following formula, and each group mean was compared to the theoretical mean μ = 1 in a one-sample *t*-test.

$$Arc^+cFos^+ / \text{chance} = \frac{\#\,Arc^+cFos^+\text{cells} \times \text{area}\,(mm^2) \times \text{cell density}\,(Hoechst^+\text{cells}/mm^2)}{\#\,Arc^+\text{cells} \times \#\,cFos^+\text{cells}}$$

To test whether IEG expression correlated with freezing levels, linear regression analyses were run independently for 1-day and 5-day retrieval, and R-squared goodness of fits were tested against the null hypotheses of slope = 0 (no relationship between variables) in each case. q-values were calculated from resultant p values and evaluated at a false discovery rate (FDR) of 0.1 within each metric, across all regions and groups analyzed, to account for multiple comparisons and limit false-positive significant correlations to a maximum of 10%. These analyses did not reveal any significant relationships between behavior and regional IEG-labeled cell counts.

Consistent with prior studies of hippocampal activity in CFC[3,6,10], sample sizes were n = 4 for the no shock group and n = 8 for encoding, 1-day retrieval, and 5-day retrieval groups each, unless otherwise noted in each figure legend, run as one cohort (no shock) or two cohorts (encoding and retrieval groups). A subset of cell counts was cross-referenced between experimenters to ensure consistency in quantification, and all experimenters were blind to the condition of tissue from each mouse within each mixed-group cohort. Allocation to experimental group was random for each mouse, including within shared housing cages, using a list randomizer. All statistical tests and p-values are listed in Supplementary Table 2.

All key resources are noted with sources and identifiers in Supplementary Table 3.

Reporting summary

Further information on research design is available in the Nature Portfolio Reporting Summary linked to this article.

Data availability

The data supporting the findings of this study are available within the paper and provided as Source data. Should raw data files be needed in another format, they are available from the corresponding author upon reasonable request.

Received: 5 September 2024; Accepted: 5 September 2025;
Published online: 09 October 2025

References

1. Wheeler, A. L. et al. Identification of a functional connectome for long-term fear memory in mice. *PLoS Comput. Biol.* **9**, e1002853 (2013).
2. Vetere, G. et al. Chemogenetic interrogation of a brain-wide fear memory network in mice. *Neuron* **94**, 363–374.e4 (2017).
3. Bonapersona, V. et al. The mouse brain after foot shock in four dimensions: Temporal dynamics at a single-cell resolution. *Proc. Natl. Acad. Sci. USA* **119**, e2114002119 (2022).
4. Semon, R. W. *The Mneme* (George Allen & Unwin Ltd., 1921).
5. Josselyn, S. A. & Tonegawa, S. Memory engrams: recalling the past and imagining the future. *Science* **367**, eaaw4325 (2020).
6. Kitamura, T. et al. Engrams and circuits crucial for systems consolidation of a memory. *Science* **356**, 73–78 (2017).
7. Tonegawa, S., Morrissey, M. D. & Kitamura, T. The role of engram cells in the systems consolidation of memory. *Nat. Rev. Neurosci.* **19**, 485–498 (2018).
8. Liu, X. et al. Optogenetic stimulation of a hippocampal engram activates fear memory recall. *Nature* **484**, 381–385 (2012).
9. Garner, A. R. et al. Generation of a synthetic memory trace. *Science* **335**, 1513–1516 (2012).
10. Denny, C. A. et al. Hippocampal memory traces are differentially modulated by experience, time, and adult neurogenesis. *Neuron* **83**, 189–201 (2014).
11. Okuno, H. Regulation and function of immediate-early genes in the brain: Beyond neuronal activity markers. *Neurosci. Res.* **69**, 175–186 (2011).
12. Minatohara, K., Akiyoshi, M. & Okuno, H. Role of immediate-early genes in synaptic plasticity and neuronal ensembles underlying the memory trace. *Front. Mol. Neurosci*. **8**, 78 (2016).
13. Chung, L. A brief introduction to the transduction of neural activity into Fos signal. *Dev. Reprod.* **19**, 61–67 (2015).
14. Gallo, F. T., Katche, C., Morici, J. F., Medina, J. H. & Weisstaub, N. V. Immediate early genes, memory and psychiatric disorders: focus on c-Fos, Egr1 and Arc. *Front. Behav. Neurosci.* **12**, 79 (2018).
15. Morgan, J. I. & Curran, T. Stimulus-transcription coupling in the nervous system: involvement of the inducible proto-oncogenes *fos* and *jun*. *Annu. Rev. Neurosci.* **14**, 421–451 (1991).
16. Guzowski, J. F., Setlow, B., Wagner, E. K. & McGaugh, J. L. Experience-dependent gene expression in the rat hippocampus after spatial learning: a comparison of the immediate-early genes *Arc*, c-*fos*, and *zif268*. *J. Neurosci.* **21**, 5089–5098 (2001).
17. Dyrvig, M. et al. Epigenetic regulation of *Arc* and *c-Fos* in the hippocampus after acute electroconvulsive stimulation in the rat. *Brain Res. Bull.* **88**, 507–513 (2012).

18. Guzowski, J. F., McNaughton, B. L., Barnes, C. A. & Worley, P. F. Environment-specific expression of the immediate-early gene *Arc* in hippocampal neuronal ensembles. *Nat. Neurosci.* **2**, 1120–1124 (1999).
19. Steward, O., Wallace, C. S., Lyford, G. L. & Worley, P. F. Synaptic activation causes the mRNA for the IEG *Arc* to localize selectively near activated postsynaptic sites on dendrites. *Neuron* **21**, 741–751 (1998).
20. Das, S., Lituma, P. J., Castillo, P. E. & Singer, R. H. Maintenance of a short-lived protein required for long-term memory involves cycles of transcription and local translation. *Neuron* **111**, 1–14 (2023).
21. Shepherd, J. D. et al. Arc/Arg3.1 mediates homeostatic synaptic scaling of AMPA receptors. *Neuron* **52**, 475–484 (2006).
22. Waung, M. W., Pfeiffer, B. E., Nosyreva, E. D., Ronesi, J. A. & Huber, K. M. Rapid translation of Arc/Arg3.1 selectively mediates mGluR-dependent LTD through persistent increases in AMPAR endocytosis rate. *Neuron* **59**, 84–97 (2008).
23. Korb, E., Wilkinson, C. L., Delgado, R. N., Lovero, K. L. & Finkbeiner, S. Arc in the nucleus regulates PML-dependent GluA1 transcription and homeostatic plasticity. *Nat. Neurosci.* **16**, 874–883 (2013).
24. Chotiner, J. K. et al. Assessment of the role of MAP kinase in mediating activity-dependent transcriptional activation of the immediate early gene *Arc/Arg3.1* in the dentate gyrus in vivo. *Learn. Mem.* **17**, 117–129 (2010).
25. Pintchovski, S. A., Peebles, C. L., Joo Kim, H., Verdin, E. & Finkbeiner, S. The serum response factor and a putative novel transcription factor regulate expression of the immediate-early gene *Arc/Arg3.1* in neurons. *J. Neurosci.* **29**, 1525–1537 (2009).
26. Kawashima, T. et al. Synaptic activity-responsive element in the *Arc/Arg3.1* promoter essential for synapse-to-nucleus signaling in activated neurons. *Proc. Natl. Acad. Sci. USA* **106**, 316–321 (2009).
27. Guzowski, J. F. et al. Inhibition of activity-dependent Arc protein expression in the rat hippocampus impairs the maintenance of long-term potentiation and the consolidation of long-term memory. *J. Neurosci.* **20**, 3993–4001 (2000).
28. Messaoudi, E. et al. Sustained Arc/Arg3.1 synthesis controls long-term potentiation consolidation through regulation of local actin polymerization in the dentate gyrus in vivo. *J. Neurosci.* **27**, 10445–10455 (2007).
29. Kyrke-Smith, M. et al. The immediate early gene Arc is not required for hippocampal long-term potentiation. *J. Neurosci.* **41**, 4202–4211 (2021).
30. Plath, N. et al. Arc/Arg3.1 is essential for the consolidation of synaptic plasticity and memories. *Neuron* **52**, 437–444 (2006).
31. Vazdarjanova, A. et al. Spatial exploration induces ARC, a plasticity-related immediate-early gene, only in calcium/calmodulin-dependent protein kinase II-positive principal excitatory and inhibitory neurons of the rat forebrain. *J. Comp. Neurol.* **498**, 317–329 (2006).
32. Pevzner, A. & Guzowski, J. F. Immediate-early gene transcriptional activation in hippocampus CA1 and CA3 does not accurately reflect rapid, pattern completion-based retrieval of context memory. *Learn. Mem.* **22**, 1–5 (2015).
33. Pastuzyn, E. D. et al. The neuronal gene *Arc* encodes a repurposed retrotransposon Gag protein that mediates intercellular RNA transfer. *Cell* **172**, 275–288.e1-e9 (2018).
34. Yassa, M. A. & Stark, C. E. L. Pattern separation in the hippocampus. *Trends Neurosci.* **34**, 515–525 (2011).
35. Tonegawa, S., Pignatelli, M., Roy, D. S. & Ryan, T. J. Memory engram storage and retrieval. *Curr. Opin. Neurobiol.* **35**, 101–109 (2015).
36. Chaaya, N., Battle, A. R. & Johnson, L. R. An update on contextual fear memory mechanisms: transition between Amygdala and Hippocampus. *Neurosci. Biobehav. Rev.* **92**, 43–54 (2018).
37. Hintiryan, H. et al. Connectivity characterization of the mouse basolateral amygdalar complex. *Nat. Commun.* **12**, 2859 (2021).
38. Smith, D. M. et al. The limbic memory circuit and the neural basis of contextual memory. *Neurobiol. Learn. Mem.* **187**, 107557 (2022).
39. Todd, T. P., Fournier, D. I. & Bucci, D. J. Retrosplenial cortex and its role in cue-specific learning and memory. *Neurosci. Biobehav. Rev.* **107**, 713–728 (2019).
40. Buckner, R. L. et al. Molecular, structural, and functional characterization of Alzheimer's disease: Evidence for a relationship between default activity, amyloid, and memory. *J. Neurosci.* **25**, 7709–7717 (2005).
41. Haberman, R. P., Koh, M. T. & Gallagher, M. Heightened cortical excitability in aged rodents with memory impairment. *Neurobiol. Aging* **54**, 144–151 (2017).
42. Le Merre, P., Ährlund-Richter, S. & Carlén, M. The mouse prefrontal cortex: Unity in diversity. *Neuron* **109**, 1925–1944 (2021).
43. Zhu, Y. et al. Dynamic salience processing in paraventricular thalamus gates associative learning. *Science* **362**, 423–429 (2018).
44. Li, Y., Dong, X., Li, S. & Kirouac, G. J. Lesions of the posterior paraventricular nucleus of the thalamus attenuate fear expression. *Front. Behav. Neurosci.* **8**, 94 (2014).
45. Hu, H., Cui, Y. & Yang, Y. Circuits and functions of the lateral habenula in health and in disease. *Nat. Rev. Neurosci.* **21**, 277–295 (2020).
46. Borzello, M. et al. Assessments of dentate gyrus function: discoveries and debates. *Nat. Rev. Neurosci.* **24**, 502–517 (2023).
47. Erwin, S. R. et al. A sparse, spatially biased subtype of mature granule cell dominates recruitment in hippocampal-associated behaviors. *Cell Rep.* **31**, 107551 (2020).
48. Zhukovskaya, A. et al. Heightened lateral habenula activity during stress produces brainwide and behavioral substrates of susceptibility. *Neuron* **112**, 3940–3956 (2024).
49. Yelhekar, T. D., Meng, M., Doupe, J. & Lin, Y. All IEGs are not created equal—molecular sorting within the memory engram. in *Engrams*, Vol. 38 (eds Gräff, J. & Ramirez, S.) (Springer International Publishing, 2024).
50. Labiner, D. M. et al. Induction of c-*fos* mRNA by kindled seizures: complex relationship with neuronal burst firing. *J. Neurosci.* **13**, 744–751 (1993).
51. Hope, B. T. et al. Induction of a long-lasting AP-1 complex composed of altered Fos-like proteins in brain by chronic cocaine and other chronic treatments. *Neuron* **13**, 1235–1244 (1994).
52. Lamothe-Molina, P. J. et al. FosB accumulation in hippocampal granule cells drives cFos pattern separation during spatial learning. *Nat. Commun.* **13**, 6376 (2022).
53. Corbett, B. F. et al. FosB regulates gene expression and cognitive dysfunction in a mouse model of Alzheimer's disease. *Cell Rep.* **20**, 344–355 (2017).
54. Griffith, E. C., West, A. E. & Greenberg, M. E. Neuronal enhancers fine-tune adaptive circuit plasticity. *Neuron* **112**, 1–15 (2024).
55. Cruz-Mendoza, F., Jauregui-Huerta, F., Aguilar-Delgadillo, A., García-Estrada, J. & Luquin, S. Immediate early gene c-fos in the brain: focus on glial cells. *Brain Sci.* **12**, 687 (2022).
56. Rodríguez, J. J. et al. ARG3.1/ARC expression in hippocampal dentate gyrus astrocytes: ultrastructural evidence and co-localization with glial fibrillary acidic protein. *J. Cell. Mol. Med.* **12**, 671–678 (2008).
57. Williamson, M. R. et al. Learning-associated astrocyte ensembles regulate memory recall. *Nature* **637**, 478–486 (2025).
58. Stone, S. S. D. et al. Functional convergence of developmentally and adult-generated granule cells in dentate gyrus circuits supporting hippocampus-dependent memory. *Hippocampus* **21**, 1348–1362 (2011).
59. Rao-Ruiz, P. et al. Engram-specific transcriptome profiling of contextual memory consolidation. *Nat. Commun.* **10**, 2232 (2019).
60. Jiang, Y. & VanDongen, A. M. J. Selective increase of correlated activity in Arc-positive neurons after chemically induced long-term potentiation in cultured hippocampal neurons. *eNeuro* **8**, ENEURO.0540-20.2021 (2021).
61. Chiaruttini, N. et al. ABBA+BraiAn, an integrated suite for whole-brain mapping, reveals brain-wide differences in immediate-early genes induction upon learning. *Cell Rep.* **44**, 115876 (2025).

62. Arai, M. et al. Combinative protein expression of immediate early genes c-Fos, Arc, and Npas4 along aversive and appetitive experience-related neural networks. *Hippocampus* **35**, e70030 (2025).
63. Ghandour, K. et al. Orchestrated ensemble activities constitute a hippocampal memory engram. *Nat. Commun.* **10**, 2637 (2019).
64. Sweis, B. M., Mau, W., Rabinowitz, S. & Cai, D. J. Dynamic and heterogeneous neural ensembles contribute to a memory engram. *Curr. Opin. Neurobiol.* **67**, 199–206 (2021).
65. Nambu, M. F., Lin, Y.-J., Reuschenbach, J. & Tanaka, K. Z. What does engram encode?: Heterogeneous memory engrams for different aspects of experience. *Curr. Opin. Neurobiol.* **75**, 102568 (2022).
66. Sun, X. et al. Functionally distinct neuronal ensembles within the memory engram. *Cell* **181**, 1–14 (2020).
67. Bahl, E. et al. Using deep learning to quantify neuronal activation from single-cell and spatial transcriptomic data. *Nat. Commun.* **15**, 779 (2024).
68. Nelson, E. D. et al. Activity-regulated gene expression across cell types of the mouse hippocampus. *Hippocampus* **33**, 1009–1027 (2023).
69. Mukherjee, D. et al. Salient experiences are represented by unique transcriptional signatures in the mouse brain. *eLife* **7**, e31220 (2018).
70. Turrigiano, G. Homeostatic synaptic plasticity: local and global mechanisms for stabilizing neuronal function. *Cold Spring Harb. Perspect. Biol.* **4**, a005736 (2012).
71. Bernier, B. E. et al. Dentate gyrus contributes to retrieval as well as encoding: Evidence from context fear conditioning, recall, and extinction. *J. Neurosci.* **37**, 6359–6371 (2017).
72. Wu, C.-H., Ramos, R., Katz, D. B. & Turrigiano, G. G. Homeostatic synaptic scaling establishes the specificity of an associative memory. *Curr. Biol.* **31**, 2274–2285 (2021).
73. Lee, I. & Kesner, R. P. Encoding versus retrieval of spatial memory: double dissociation between the dentate gyrus and the perforant path inputs into CA3 in the dorsal hippocampus. *Hippocampus* **14**, 66–76 (2004).
74. Bailey, D. J. & Wade, J. Differential expression of the immediate early genes FOS and ZENK following auditory stimulation in the juvenile male and female zebra finch. *Mol. Brain Res.* **116**, 147–154 (2003).
75. Stack, A. et al. Sex differences in social interaction in rats: role of the immediate-early gene zif268. *Neuropsychopharmacology* **35**, 570–580 (2010).
76. Yagi, S., Chow, C., Lieblich, S. E. & Galea, L. A. M. Sex and strategy use matters for pattern separation, adult neurogenesis, and immediate early gene expression in the hippocampus. *Hippocampus* **26**, 87–101 (2016).
77. Yagi, S. et al. Sex and estrous cycle differences in immediate early gene activation in the hippocampus and the dorsal striatum after the cue competition task. *Horm. Behav.* **87**, 69–79 (2017).
78. Ma, Q., Wonnacott, S., Bailey, S. J. & Bailey, C. P. Sex differences in brain region-specific activation of c-fos following kappa opioid receptor stimulation or acute stress in mice. *Int. J. Mol. Sci.* **24**, 15098 (2023).
79. Zhang, K. et al. The sexually divergent cFos activation map of fear extinction. *Heliyon* **10**, e23748 (2024).
80. McKhann II et al. Mouse strain differences in kainic acid sensitivity, seizure behavior, mortality, and hippocampal pathology. *Neuroscience* **122**, 551–561 (2003).
81. Pavlova, I. P., Shipley, S. C., Lanio, M., Hen, R. & Denny, C. A. Optimization of immunolabeling and clearing techniques for indelibly labeled memory traces. *Hippocampus* **28**, 523–535 (2018).
82. Schindelin, J. et al. Fiji: an open-source platform for biological-image analysis. *Nat. Methods* **9**, 676–682 (2012).
83. Allen Institute for Brain Science (2004). Allen Mouse Brain Atlas [dataset]. Available from http://atlas.brain-map.org. Allen Institute for Brain Science (2011).

Acknowledgements

We thank members of the Denny Laboratory for their insightful comments on this project and manuscript. Select graphics were created in BioRender. N.E.B. was supported by the National Science Foundation Graduate Research Fellowship Program (NSF GRFP) DGE 2036197 and an F31 AG090071. L.I.Q. was supported by the Barnard Summer Research Institute (SRI). M.S. was supported by an F99 NS129178, an F31 MH125656, and a Neurobiology & Behavior (NB&B) Research Training Grant T32 HD007430. C.A.D. was supported by a retention package from the NYSPI and an R01 HD101402.

Author contributions

N.E.B. conceived of and designed the study, acquired, analyzed, and interpreted the data, drafted the work, and revised it critically for intellectual content. L.I.Q. acquired and analyzed the data and contributed to drafting the work. M.S. conceived of and designed the study and contributed to data acquisition. C.A.D. conceived of and designed the study, interpreted the data, and revised the work critically for intellectual content. All authors approved the version of the manuscript to be published and agreed to be accountable for all aspects of the work. All authors commit to ensuring that questions related to the accuracy and integrity of any part of the work are appropriately investigated and resolved.

Competing interests

N.B., L.Q. and M.S. declare no competing interests. C.A.D. is named on provisional, non-provisional, and awarded patent applications for the prophylactic use of (*R*, *S*)-ketamine and related compounds against stress-related psychiatric disorders; however, these patents are not applicable to this study, and C.A.D. therefore declares no competing interests.

Additional information

Supplementary information The online version contains supplementary material available at https://doi.org/10.1038/s42003-025-08856-5.

Correspondence and requests for materials should be addressed to Christine A. Denny.

Peer review information *Communications Biology* thanks the anonymous reviewers for their contribution to the peer review of this work. Primary handling editors: Benjamin Bessieres.